Supplement of Earth Syst. Dynam., 16, 1739–1758, 2025 https://doi.org/10.5194/esd-16-1739-2025-supplement © Author(s) 2025. CC BY 4.0 License.





Supplement of

AR6 updates to RF by GHGs and aerosols lower the probability of accomplishing the Paris Agreement compared to AR5 formulations

Endre Z. Farago et al.

Correspondence to: Endre Z. Farago (efarago@umd.edu) and Ross J. Salawitch (rsalawit@umd.edu)

The copyright of individual parts of the Supplement might differ from the article licence.

Section S1

10

25

We provide a summary of the ERF formulations that are used to compute ERF due to GHGs for the Baseline and AR6 frameworks in Table S1. The coefficients used in the equations of Table S1 are listed in Table S2. Table S3 summarizes the central, 1σ and 2σ values for ERF_{AER} of the Gaussians that are used weight the EM–GC ensemble. These numerical values correspond to the highlighted points on the Gaussians shown in Figure 1a–b and are derived from the best estimates and ranges of ERF_{AER} from IPCC, which are shown in Table S3. For the Baseline framework, the 1σ boundaries of the Gaussian were set to match the IPCC AR5 "likely range" of ERF_{AER}, while the 2σ boundaries are based on the AR5 range. For the AR6 framework, the 2σ boundaries are from the AR6 range for ERF_{AER} in 2019, while the 1σ boundaries were determined to be halfway between the 2σ ERF_{AER} and the IPCC central estimate (Table S3).

Equations S1–S3 show the computation of the three separate χ^2 values, which are used to quantify the goodness of the fit to the historical GMST and OHC record for a given combination of λ_{Σ} and ERF_{AER}. In Eqs. S1–S3, $<\Delta T_{OBS}>$, $<\Delta T_{MDL}>$ and $<\sigma_{OBS}>$ correspond to the annually averaged observed and modeled GMST anomaly, and the observational uncertainty of the GMST record, respectively. Annual averages are used instead of monthly values because the autocorrelation functions of measured and modeled ΔT display similar shapes using annual averages and do not match utilizing monthly averages, as described in the Supplement of Canty et al. (2013) and Sect. 2.1 of McBride et al. (2021). More details on the computation of χ^2 values are provided in Sect. 2.1 of McBride et al. (2021).

Figure S1 shows the temporal evolution of the concentration (Fig S1a-c) and ERF (Fig. S1d-f) of CO₂, CH₄, and N₂O for the Baseline (dashed lines) and AR6 (solid lines) frameworks. as well as ERF from tropospheric aerosols (ERF_{AER}), the total ERF from all GHGs, and ERF from overall anthropogenic activity (Fig. S1g-i). Markers on the vertical axis in Fig. S1i correspond to the nameplate RF levels associated with each SSP scenario.

Figure S2 provides a visual depiction of the ERF_{AER} ensemble within EM-GC, obtained by scaling the IPCC best-estimate time series (thick black line) by a series of constant multiplicative factors, as described in Sect. 2.1.3. The colors of individual lines correspond to the value of ERF_{AER,2019} for each time series, as indicated by the color bar. Not all members of the ensemble are shown, to avoid visual clutter.

Figure S3 shows the probability distribution functions (PDFs) of AAWR and EffCS from the weighted EM–GC simulations. The height of bars on Fig. S3 corresponds to the probability of AAWR (Fig. S3a) and EffCS (Fig. S3b) being in the range defined by the width of each column. Values of the median and 5–95% range for AAWR and EffCS are also shown at the top of each panel.

Figures S4 and S5 show the values of ΔT_{2100} as the function of climate feedback (vertical axis) and the strength of aerosol cooling (horizontal axis) in a manner similar to Fig. 1, for the Baseline and AR6 frameworks, respectively. Colors correspond to values of ΔT_{2100} , and are only shown for the ensemble members which satisfy all three reduced χ^2 constraints described in Sect. 2.2.2 and given in Eqs. S1–S3.

Figure S6 shows the time-dependent GMST forecast for the Baseline Framework. This figure is analogous to Fig. 3 of the main paper, where the time-dependent GMST projections are shown for the AR6 framework. Projected times of crossing the 1.5 $^{\circ}$ C and 2.0 $^{\circ}$ C thresholds at 5%, 50% and 95% probabilities are shown with gold circles. The crossover years marked in Fig. S6 are listed in Table 3 of the main paper. The minimum, maximum and multi-model mean of Δ T from CMIP6 ESMs are also shown with grey lines, in the same manner as Fig. 3.

Table S1: Formulations of SARF, and tropospheric adjustments used to compute ERF for the Baseline and AR6 frameworks. C, M and N represent the concentrations of CO₂, CH₄ and N₂O, respectively, at a given time. C₀, M₀ and N₀ are the pre–industrial concentrations of these three GHGs. Values of C₀, M₀ and N₀ used in this study are listed in Table S2. Coefficients used in the SARF formulations are also listed in Table S2.

Framework	GHG	CADE Estimate	Trop.	Primary	
Framework		SARF Formula		References	
Baseline	CO ₂	$SARF = \alpha_{CO2} \ln(\frac{C}{C_0})$	None		
	CH4	$SARF = \alpha_{CH4} \left(\sqrt{M} - \sqrt{M_0} \right) - (f(M, N_0) - f(M_0, N_0))$ where $f(M, N) = 0.47 \ln (1 + 2.01 \times 10^{-5} (MN)^{0.75} + 5.31 \times 10^{-15} \times M(MN)^{1.52})$	None	(Myhre et al., 1998; Myhre et	
	N ₂ O	$SARF = \alpha_{N20} \left(\sqrt{N} - \sqrt{N_0} \right) - (f(M_0, N) - f(M_0, N_0))$ where $f(M, N) = 0.47 \ln (1 + 2.01 \times 10^{-5} (MN)^{0.75} + 5.31 \times 10^{-15} \times M(MN)^{1.52})$	None	al., 2013b)	
AR6	CO ₂	$C_{\alpha_{max}} = C_0 - \frac{b_1}{2a_1}$ $\alpha' = \begin{cases} d_1 - \frac{b_1^2}{4a_1} & \text{if } C > C_{\alpha_{max}} \\ d_1 + a_1(C - C_0)^2 + b_1(C - C_0) & \text{if } C_0 < C < C_{\alpha_{max}} \\ d_1 & \text{if } C < C_0 \end{cases}$ $\alpha_{N2O} = C_1 \times \sqrt{N}$ $SARF = (\alpha' + \alpha_{N2O}) \times \ln(\frac{C}{C_0})$		(Meinshausen et al., 2020; Forster et al., 2021; Smith et al., 2021)	
	CH ₄	$SARF = (a_3\sqrt{M} + b_3\sqrt{N} + d_3)(\sqrt{M} - \sqrt{M_0})$	-14%		
	N ₂ O	$SARF = (a_2\sqrt{C} + b_2\sqrt{N} + c_2\sqrt{M} + d_2)(\sqrt{N} - \sqrt{N_0})$	+7%		

Table S2: Coefficients and pre-industrial concentrations of GHGs used in the formulations listed in Table S1 for the computation of SARF and ERF in this study.

Framework	GHG	SARF Coefficients	Primary References		
Baseline	CO ₂	$\alpha_{\rm CO2} = 5.35 \; \rm W \; m^{-2}$	(Myhre et al., 1998; Myhre		
		$C_0=278 \text{ ppm}$			
		$\alpha_{\text{CH4}} = 0.036 \text{ W m}^{-2} \text{ ppb}^{-1/2}$			
	CH4	M ₀ = 722 ppb	et al., 2013a; Myhre et al.,		
		$N_0=270 \text{ ppb}$	2013b)		
	N ₂ O	$\alpha_{\rm N2O} = 0.12~{\rm W}~{\rm m}^{-2}~{\rm ppb}^{-1/2}$	20130)		
		M ₀ = 722 ppb			
		$N_0=270 \text{ ppb}$			
	CO ₂	$a_1 = -2.4785 \times 10^{-7} \text{ W m}^{-2} \text{ ppm}^{-2}$			
		$b_1 = 7.5906 \times 10^{-4} \text{ W m}^{-2} \text{ ppm}^{-1}$			
		$c_1 = -2.1492 \times 10^{-3} \text{ W m}^{-2} \text{ ppb}^{-1/2}$			
		$d_1 = 5.2488 \text{ W m}^{-2}$			
		$C_0 = 278.3 \text{ ppm}$			
	CH ₄	$a_3 = -8.9603 \times 10^{-5} \text{ W m}^{-2} \text{ ppb}^{-1}$	(Meinshausen et al., 2020;		
AR6		$b_3 = -1.2462 \times 10^{-4} \text{ W m}^{-2} \text{ ppb}^{-1}$	Forster et al., 2021; Smith et		
		$c_3 = 0.045194 \text{ W m}^{-2} \text{ ppb}^{-1/2}$	al., 2021)		
		M ₀ = 729 ppb			
	N ₂ O	$a_2 = -3.4197 \times 10^{-4} \text{ W m}^{-2} \text{ ppm}^{-1/2} \text{ ppb}^{-1/2}$			
		$b_2 = 2.5455 \times 10^{-4} \text{ W m}^{-2} \text{ ppb}^{-1}$			
		$c_2 = -2.4357 \times 10^{-4} \text{ W m}^{-2} \text{ ppb}^{-1}$			
		$d_2 = 0.12173 \text{ W m}^{-2} \text{ ppb}^{-1/2}$			
		$N_0 = 270.1 \text{ ppb}$			

Table S3: Central values, 1σ and 2σ boundaries of the Gaussians used to weight the EM-GC output for the Baseline and AR6 frameworks. Values shown in this table are marked by circles on the Gaussians in Fig. 1a-b.

		ERFAER,t (W m ⁻²)						
Framework	Reference year (t)	2σ	1σ	Central	1σ	2σ	Corresponding IPCC Range	Primary References
Baseline	2011	-0.1	-0.4	-0.9	-1.5	-1.9	-0.9 [-0.1 to -1.9] (AR5 range) and [-0.4 to -1.5] (AR5 "likely" range)	(Myhre et al., 2013b)
AR6	2019	-0.4	-0.75	-1.1	-1.4	-1.7	-1.1 [-0.4 to -1.7] (AR6 range)	(Forster et al., 2021)

$$\chi^{2}_{ATM} = \frac{1}{N_{YEARS} - N_{FITTING PARAMETERS} - 1} \times \sum_{j=1}^{N_{YEARS}} \frac{1}{\langle \sigma_{OBS} \rangle^{2}} (\langle \Delta T_{OBS,j} \rangle - \langle \Delta T_{MDL,j} \rangle)^{2}$$
 (S1)

$$\chi^{2}_{RECENT} = \frac{1}{N_{YEARS,REC} - N_{FITTING\ PARAMETERS} - 1} \times \sum_{j=1}^{N_{YEARS,REC}} \frac{1}{\langle \sigma_{OBS} \rangle^{2}} (\langle \Delta T_{OBS,j} \rangle - \langle \Delta T_{MDL,j} \rangle)^{2}$$
 (S2)

$$\chi^{2}_{OCEAN} = \frac{1}{N_{YEARS,OHC} - N_{FITTING\ PARAMETERS} - 1} \times \sum_{j=1}^{N_{YEARS,OHC}} \frac{1}{\langle \sigma_{OBS} \rangle^{2}} (\langle \text{OHC}_{OBS,j} \rangle - \langle \text{OHC}_{MDL,j} \rangle)^{2}$$
 (S3)

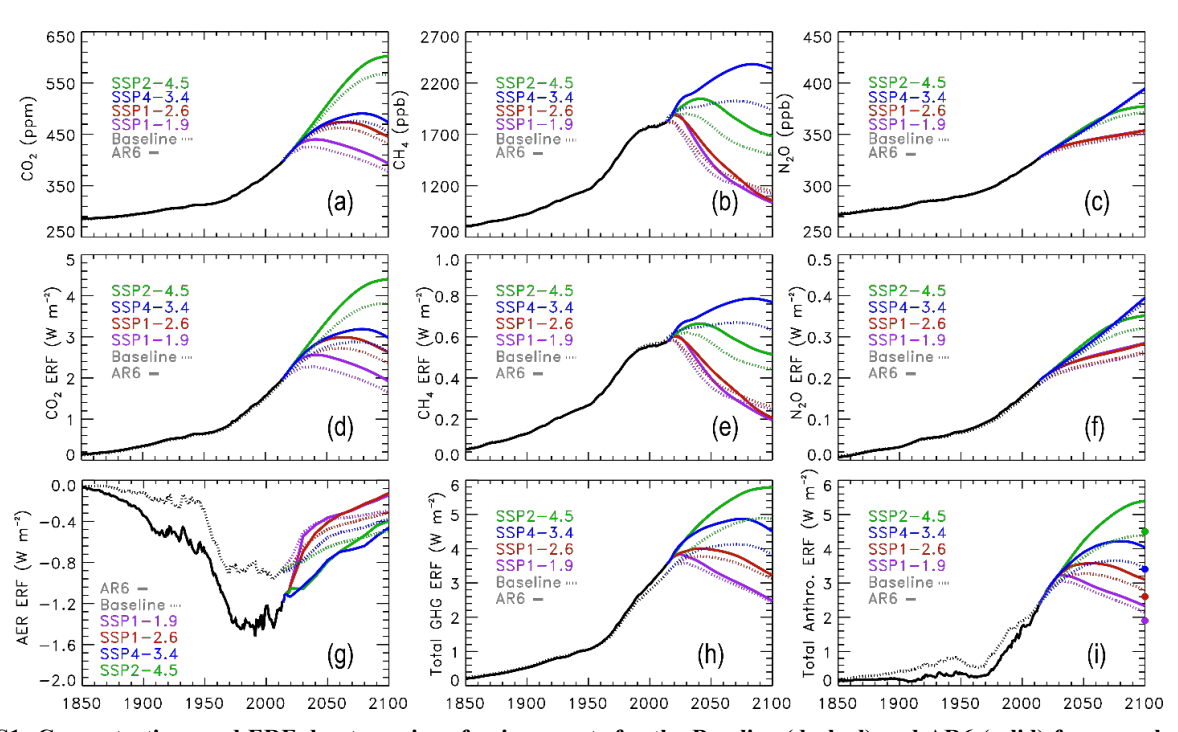


Figure S1: Concentrations and ERF due to various forcing agents for the Baseline (dashed) and AR6 (solid) frameworks. Colors represent SSP scenarios, as indicated on the individual panels. (a) Concentration of CO₂. (b) Concentration of CH₄. (c) Concentration of N₂O. (d) ERF from CO₂. (e) ERF from CH₄, including ERF from the enhancement of stratospheric water vapor due to methane. (f) ERF from N₂O. (g) ERF due to tropospheric aerosols. (h) ERF from all GHGs, including halogens and tropospheric O₃, as well as land-use change. (i) Total anthropogenic ERF. Colored circles on the right-hand axis represent the nameplate RF associated with each SSP scenario.

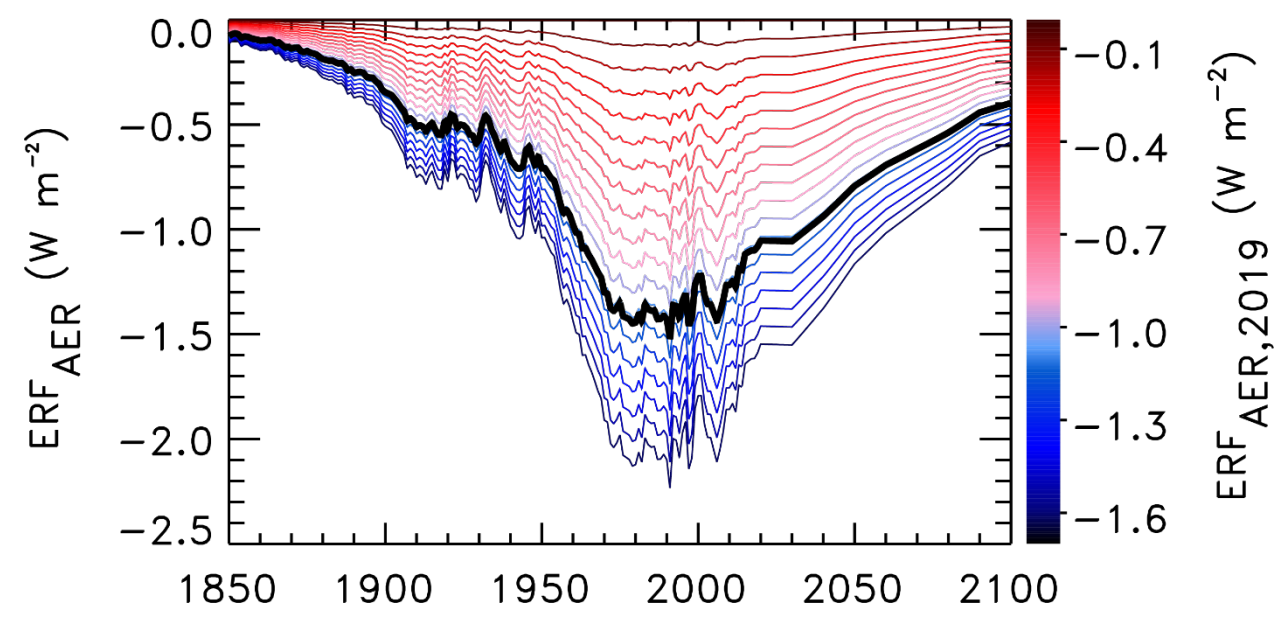
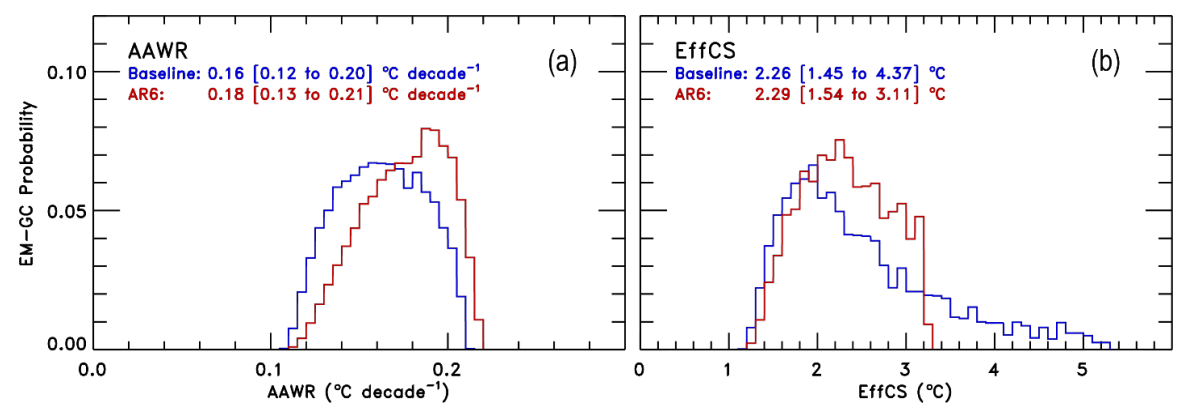


Figure S2: Visual depiction of the EM-GC ERF_{AER} ensemble used in the AR6 Framework, generated by the scaling of the IPCC-prescribed timeseries of ERF_{AER} from Annex III of AR6 (IPCC, 2021) as described in Sect. 2.1.3. The solid black line corresponds to the "best estimate" time series that is scaled to obtain the ensemble. For this figure, beyond 2019, the SSP2-4.5 time series was scaled. Colors denote ERF_{AER} in 2019 as indicated by the color bar. Not all ensemble members are shown, to avoid visual clutter.



75 Figure S3: (a) Probability distribution functions (PDFs) of AAWR for the Baseline framework (blue) and the AR6 framework (red). The EM-GC median (defined as the 50th percentile probability), and 5th to 95th percentile range is displayed at the top. (b) PDFs of EffCS within the Baseline (blue) and AR6 framework (red), with the corresponding median and range.

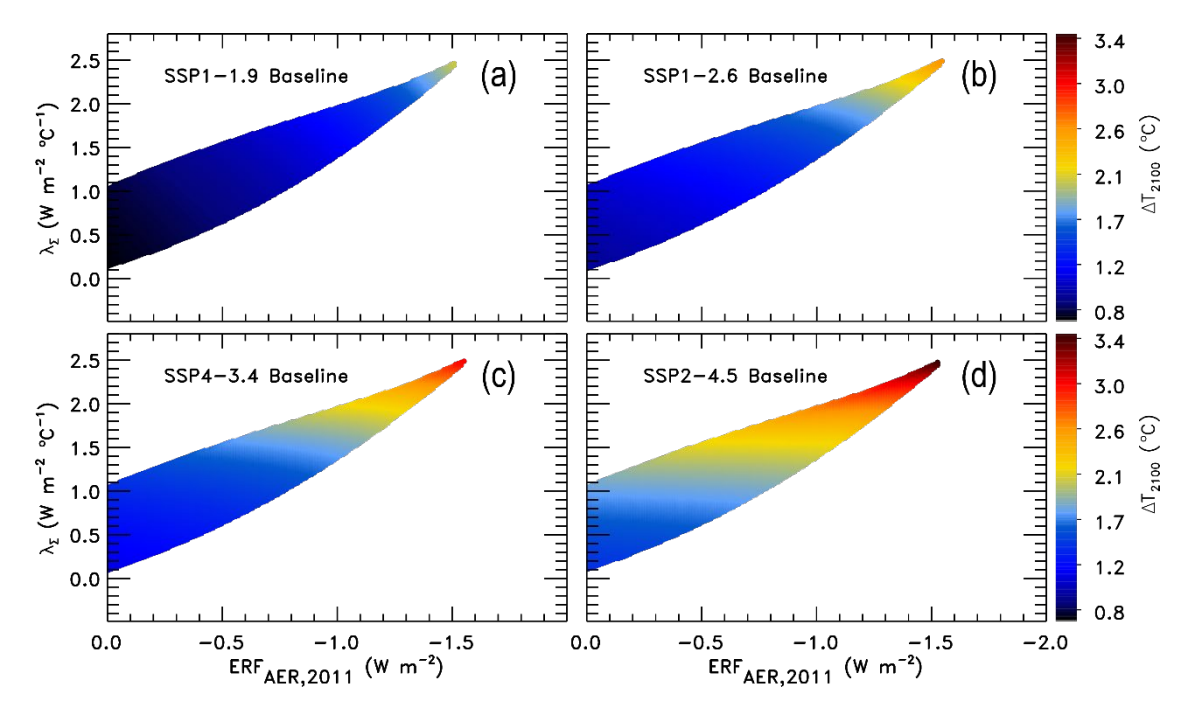


Figure S4: GMST anomaly at the end of the century (ΔT_{2100}) relative to a pre-industrial baseline, as the function of climate feedback (vertical axis) and the strength of aerosol cooling (horizontal axis) for the Baseline framework. Colors denote values of ΔT_{2100} as indicated by the color bars on the right, which is shown only for ensemble members that yield a good fit to the observed GMST and OHC record. (a) ΔT_{2100} for SSP1-1.9. (b) ΔT_{2100} for SSP1-2.6. (c) ΔT_{2100} for SSP4-3.4. (d) ΔT_{2100} for SSP2-4.5.

80

85

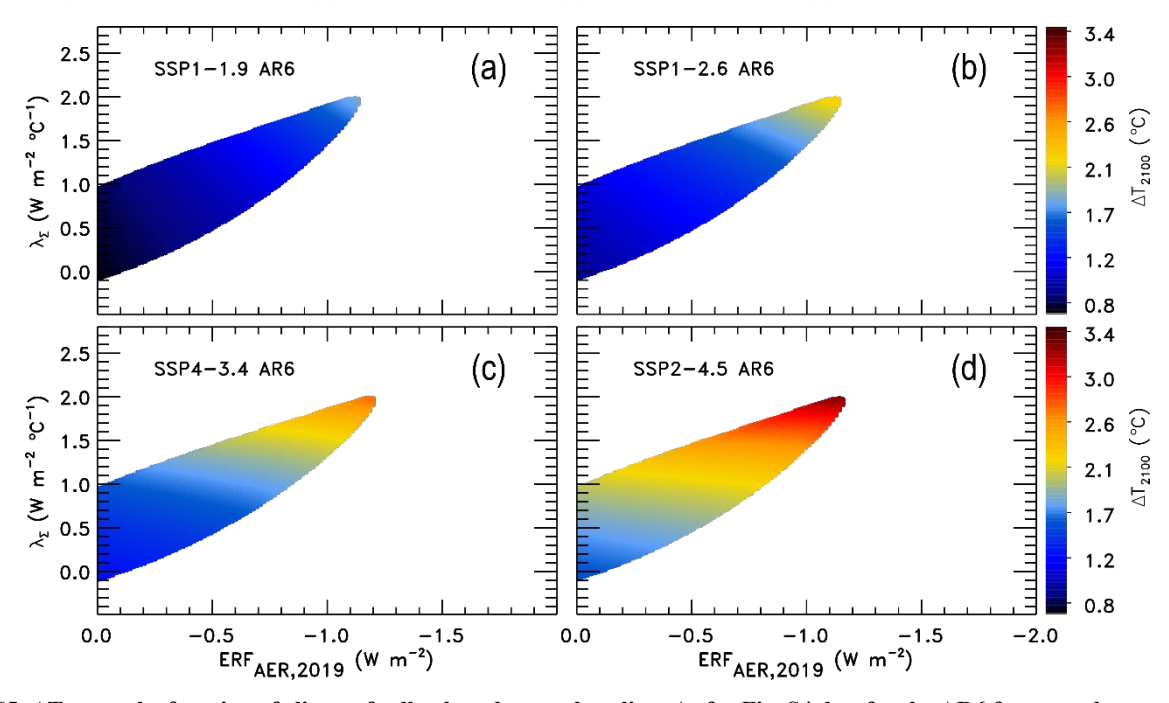


Figure S5: ΔT₂₁₀₀ as the function of climate feedback and aerosol cooling. As for Fig. S4, but for the AR6 framework.

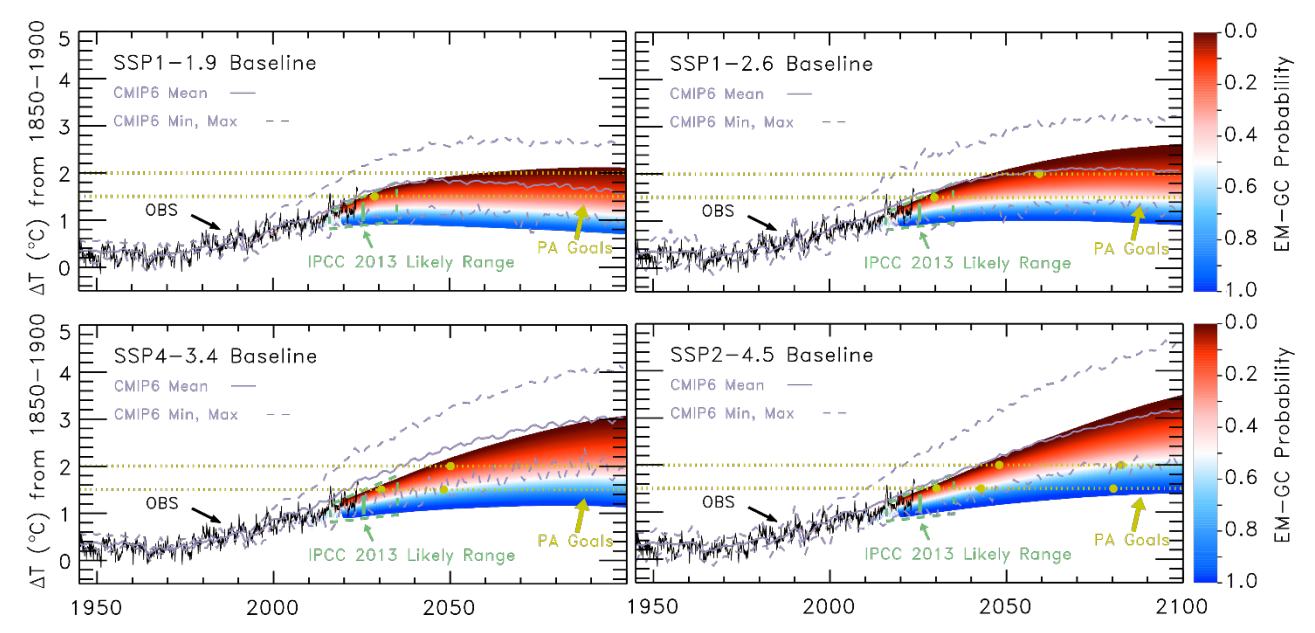


Figure S6: Time-dependent probabilistic forecast of ΔT. As for Fig. 3 of the main paper, but for the Baseline framework.

References

Canty, T., Mascioli, N. R., Smarte, M. D., and Salawitch, R. J.: An empirical model of global climate-Part 1: A critical evaluation of volcanic cooling, Atmospheric Chemistry and Physics, 13, 10.5194/acp-13-3997-2013, 2013.

95 Forster, P. M., Storelvmo, T., Armour, K., Collins, W., Dufresne, J. L., Frame, D., Lunt, D. J., Mauritsen, T., Palmer, M. D., Watanabe, M., Wild, M., and Zhang, H.: Chapter 7: The Earth's Energy Budget, Climate Feedbacks, and Climate Sensitivity, Climate Change 2021: The Physical Science Basis. Contribution of Working Group I to the Sixth Assessment Report of the Intergovernmental Panel on Climate Change, 2021.

IPCC: Annex III: Tables of historical and projected well-mixed greenhouse gas mixing ratios and effective radiative forcing of all climate forcers [Dentener F.J., B. Hall, C. Smith (eds.)], in: Climate Change 2021: The Physical Science Basis. Contribution of Working Group I to the Sixth Assessment Report of the Intergovernmental Panel on Climate Change, edited by: Masson-Delmotte, V., Zhai, P., Pirani, A., Connors, S. L., Péan, C., Berger, S., Caud, N., Chen, Y., Goldfarb, L., Gomis, M. I., Huang, M., Leitzell, K., Lonnoy, E., Matthews, J. B. R., Maycock, T. K., Waterfield, T., Yelekçi, O., Yu, R., and Zhou, B., Cambridge University Press, Cambridge, United Kingdom and New York, NY, USA, 2139–2152, 10.1017/9781009157896.017, 2021.

Kirtman, B., Power, S. B., Adedoyin, J. A., Boer, G. J., Bojariu, R., Camilloni, I., Doblas-Reyes, F. J., Fiore, A. M., Kimoto, M., Meehl, G. A., Prather, M., Sarr, A., Schär, C., Sutton, R., van Oldenborgh, G. J., Vecchi, G., and Wang, H. J.: Near-term Climate Change: Projections and Predictability. In: Climate Change 2013: The Physical Science Basis. Contribution of Working Group I to the Fifth Assessment Report of the Intergovernmental Panel on Climate Change [Stocker, T.F., D. Qin, G.-K. Plattner, M. Tignor, S.K. Allen, J. Boschung, A. Nauels, Y. Xia, V. Bex and P.M. Midgley (eds.)]. doi:10.1017/CBO9781107415324.023, 2013.

- McBride, L. A., Hope, A. P., Canty, T. P., Bennett, B. F., Tribett, W. R., and Salawitch, R. J.: Comparison of CMIP6 historical climate simulations and future projected warming to an empirical model of global climate, Earth Syst. Dynam., 12, 545-579, 10.5194/esd-12-545-2021, 2021.
- Meinshausen, M., Nicholls, Z. R. J., Lewis, J., Gidden, M. J., Vogel, E., Freund, M., Beyerle, U., Gessner, C., Nauels, A., Bauer, N., Canadell, J. G., Daniel, J. S., John, A., Krummel, P. B., Luderer, G., Meinshausen, N., Montzka, S. A., Rayner, P. J., Reimann, S., Smith, S. J., Van Den Berg, M., Velders, G. J. M., Vollmer, M. K., and Wang, R. H. J.: The shared socioeconomic pathway (SSP) greenhouse gas concentrations and their extensions to 2500, Geoscientific Model Development, 13, 10.5194/gmd-13-3571-2020, 2020.
- Myhre, G., Highwood, E. J., Shine, K. P., and Stordal, F.: New estimates of radiative forcing due to well mixed greenhouse gases, Geophysical Research Letters, 25, 10.1029/98GL01908, 1998.
 - Myhre, G., Shindell, D., Bréon, F.-M., Collins, W., Fuglestvedt, J., Huang, J., Koch, D., Lamarque, J.-F., Lee, D., Mendoza, B., Nakajima, T., Robock, A., Stephens, G., Takemura, T., and Zhang, H.: Anthropogenic and Natural Radiative Forcing Supplementary Material. In: Climate Change 2013: The Physical Science Basis. Contribution of Working Group I to the Fifth
- Assessment Report of the Intergovernmental Panel on Climate Change [Stocker, T.F., D. Qin, G.-K. Plattner, M. Tignor, S.K. Allen, J. Boschung, A. Nauels, Y. Xia, V. Bex and P.M. Midgley (eds.)]. 2013a.
 - Myhre, G., Shindell, D., Bréon, F. M., Collins, W. D., Fuglestvedt, J., Huang, J., Koch, D., Lamarque, J. F., Lee, D., Mendoza, B., Nakajima, T., Robock, a., Stephens, G., Takemura, T., and Zhan, H.: IPCC AR5 (2013) Chapter 8: Anthropogenic and Natural Radiative Forcing, in: Climate Change 2013: The Physical Science Basis. Contribution of Working Group I to the Fifth
- 130 Assessment Report of the Intergovernmental Panel on Climate Change, 2013b.
 - Smith, C., Nicholls, Z. R. J., Armour, K., Collins, W., Forster, P., Meinshausen, M., Palmer, M. D., and Watanabe, M.: The Earth's Energy Budget, Climate Feedbacks, and Climate Sensitivity Supplementary Material. In Climate Change 2021: The Physical Science Basis. Contribution of Working Group I to the Sixth Assessment Report of the Intergovernmental Panel on Climate Change [Masson-Delmotte, V., P. Zhai, A. Pirani, S.L. Connors, C. Péan, S. Berger, N. Caud, Y. Chen, L. Goldfarb,
- M.I. Gomis, M. Huang, K. Leitzell, E. Lonnoy, J.B.R. Matthews, T.K. Maycock, T. Waterfield, O. Yelekçi, R. Yu, and B. Zhou (eds.)]. Available from https://www.ipcc.ch/, 2021.